data

MDPI

Data Descriptor

OSBA: An Open Neonatal Neuroimaging Atlas and Template for Spina Bifida Aperta

Anna Speckert [1,2], Hui Ji [1], Kelly Payette [1], Patrice Grehten [3,4], Raimund Kottke [3,4], Samuel Ackermann [1], Beth Padden [5,6], Luca Mazzone [6,7], Ueli Moehrlen [6,7,8], Spina Bifida Study Group Zurich [9,†] and Andras Jakab [1,2,8,*]

1 Center for MR-Research, University Children's Hospital Zurich, 8032 Zurich, Switzerland; anna.speckert@kispi.uzh.ch (A.S.); hui.ji@kispi.uzh.ch (H.J.); kelly.payette@kispi.uzh.ch (K.P.); samuel.ackermann@kispi.uzh.ch (S.A.)
2 University Research Priority Program (URPP), Adaptive Brain Circuits in Development and Learning (AdaBD), University of Zurich, 8057 Zurich, Switzerland
3 Department of Diagnostic Imaging, University Children's Hospital Zurich, 8032 Zurich, Switzerland; patrice.grehten@kispi.uzh.ch (P.G.); raimund.kottke@kispi.uzh.ch (R.K.)
4 The Zurich Center for Fetal Diagnosis and Therapy, University Children's Hospital Zurich, 8032 Zurich, Switzerland
5 Division of Pediatric Rehabilitation, University Children's Hospital Zurich, 8032 Zurich, Switzerland; beth.padden@kispi.uzh.ch
6 Zurich Center for Spina Bifida, University Children's Hospital Zurich, 8032 Zurich, Switzerland; luca.mazzone@kispi.uzh.ch (L.M.); ueli.moehrlen@kispi.uzh.ch (U.M.)
7 Department of Pediatric Surgery, University Children's Hospital Zurich, 8032 Zurich, Switzerland
8 Faculty of Medicine, University of Zurich, 8057 Zurich, Switzerland
9 Spina Bifida Study Group Zurich, Zurich, Switzerland; sba@kispi.uzh.ch
* Correspondence: andras.jakab@kispi.uzh.ch; Tel.: +41-44-266-3129
† All members are listed in the Acknowledgements section.

check for updates

Citation: Speckert, A.; Ji, H.; Payette, K.; Grehten, P.; Kottke, R.; Ackermann, S.; Padden, B.; Mazzone, L.; Moehrlen, U.; Spina Bifida Study Group Zurich; et al. OSBA: An Open Neonatal Neuroimaging Atlas and Template for Spina Bifida Aperta. *Data* **2024**, *9*, 107. https://doi.org/10.3390/data9090107

Academic Editor: Sameer Antani

Received: 25 June 2024
Revised: 13 September 2024
Accepted: 16 September 2024
Published: 17 September 2024

Copyright: © 2024 by the authors. Licensee MDPI, Basel, Switzerland. This article is an open access article distributed under the terms and conditions of the Creative Commons Attribution (CC BY) license (https://creativecommons.org/licenses/by/4.0/).

Abstract: We present the Open Spina Bifida Aperta (OSBA) atlas, an open atlas and set of neuroimaging templates for spina bifida aperta (SBA). Traditional brain atlases may not adequately capture anatomical variations present in pediatric or disease-specific cohorts. The OSBA atlas fills this gap by representing the computationally averaged anatomy of the neonatal brain with SBA after fetal surgical repair. The OSBA atlas was constructed using structural T2-weighted and diffusion tensor MRIs of 28 newborns with SBA who underwent prenatal surgical correction. The corrected gestational age at MRI was 38.1 ± 1.1 weeks (mean ± SD). The OSBA atlas consists of T2-weighted and fractional anisotropy templates, along with nine tissue prior maps and region of interest (ROI) delineations. The OSBA atlas offers a standardized reference space for spatial normalization and anatomical ROI definition. Our image segmentation and cortical ribbon definition are based on a human-in-the-loop approach, which includes manual segmentation. The precise alignment of the ROIs was achieved by a combination of manual image alignment and automated, non-linear image registration. From the clinical and neuroimaging perspective, the OSBA atlas enables more accurate spatial standardization and ROI-based analyses and supports advanced analyses such as diffusion tractography and connectomic studies in newborns affected by this condition.

Keywords: spina bifida aperta; neonatal atlas; T2-weighted MRI; diffusion MRI

1. Summary

Neuroimaging atlases are indispensable for image analysis. They consist of templates that represent common features of the human brain by averaging the brain anatomy of a population [1], as well as maps representing semantic neuroanatomical labels. In the field of neuroimaging analysis, the most common source for constructing atlases are MR images from a group of individuals representative of the group the atlas is meant to represent.

These images are then spatially normalized to a common coordinate system through registration and fusion methods. Atlases are particularly useful for carrying out group-level measurements in a subject cohort after spatial normalization, measuring variability in brain anatomy, and establishing localization in functional experiments. Atlases are particularly useful for multi-center studies [1,2].

However, atlases designed for the general population might not be suitable for specific groups, such as pediatric or disease-specific populations [3]. This has led to the development of more tailored atlases for such populations [3]. This remains a challenge for the developing brain, where extensive anatomical changes take place in a short period of time, requiring age-specific atlases [4,5]. Having only age-specific atlases is insufficient when fetal or neonatal brain anatomy diverges from normal development or for diseases such as open spina bifida or spina bifida aperta (SBA), one of the most prevalent fetal abnormalities affecting the central nervous system [6]. Fidon [2] confronted this challenge and developed a spatio-temporal fetal brain atlas for SBA.

SBA manifests when the neural tube does not successfully close within the first four weeks following conception [2]. SBA manifests in multiple brain malformations, most frequently an abnormal corpus callosum, hypoplastic pons, enlargement of the ventricles, cerebellar malformation, and hypoplastic mesencephalon [7]. These characteristic anatomical differences are depicted in Figure 1, which compares the averaged T2-weighted images of healthy neonates and those with SBA. Spatially normalizing MR images for neuroimaging analysis is particularly challenging when dealing with subjects whose anatomical structures are underdeveloped, malformed, or enlarged to varying degrees, as accurately establishing correspondences becomes inherently difficult in these cases. Not only is the fetal period of SBA crucial to study, but so is the neonatal phase. The most frequently reported anomalies during this stage, as highlighted by Mufti's [8] review, are callosal dysgenesis and heterotopia. These anomalies are likely linked to disruptions in neural migration, influenced by the altered CSF dynamics in SBA [9]. The challenge when studying neonatal SBA brains lies in the lack of temporal and disease-specific atlases that could provide anatomical context to the MR images. While there are neonatal atlases available for typically developing brains, such as the Edinburgh Neonatal Atlas (ENA33), which parcellates the brain into 107 anatomical regions and is created through temporal back-propagation of the widely used adult brain atlas (SRI24/TZO) to the neonatal date [10], dedicated neonatal atlases for SBA analysis are currently unavailable. Relying on healthy neonatal atlases for SBA analysis poses a challenge due to the ambiguous mapping between regions of interest (ROI) to SBA brains, marked by heterotopia, callosal dysgenesis, and enlarged ventricles.

Here, we present a new, open atlas and set of neuroimaging templates for SBA, grounded in the ENA33 atlas, enabling direct comparisons and supporting future research on neonates with SBA. The Open Spina Bifida Aperta (OSBA) atlas addresses this gap, namely, a need for a dedicated neonatal SBA atlas that ideally aligns with those designed for healthy neonatal brains, facilitating case-control studies. The OSBA atlas was constructed using widely-used normalization and atlas creation tools and comprised T2-weighted and diffusion tensor MRI-based templates of newborns with SBA. The anatomical label maps comprise tissue prior maps and ROIs according to the definition of the ENA33 atlas. The OSBA atlas is a valuable tool for spatial standardization in SBA and for a wide range of applications where ROIs are necessary for defining anatomical regions for between-subject statistical analysis. An example is studying the connectivity structure of the newborn brain with SBA. In such studies, the OSBA atlas would provide a joint reference space for spatial normalization as well as ROIs to define the seeds for diffusion tractography and, consequently, the nodes for connectomic analysis. The OSBA atlas would also support clinical research by improving the accuracy of neuroimaging studies in SBA populations, facilitating the identification of structural brain abnormalities, and enhancing region-based analyses. For example, improving the spatial accuracy during automated, ROI-based analysis in SBA populations. Thus, the OSBA atlas serves not only as a technical

advancement but also as a practical tool with significant implications for research and clinical outcomes in the context of spina bifida.

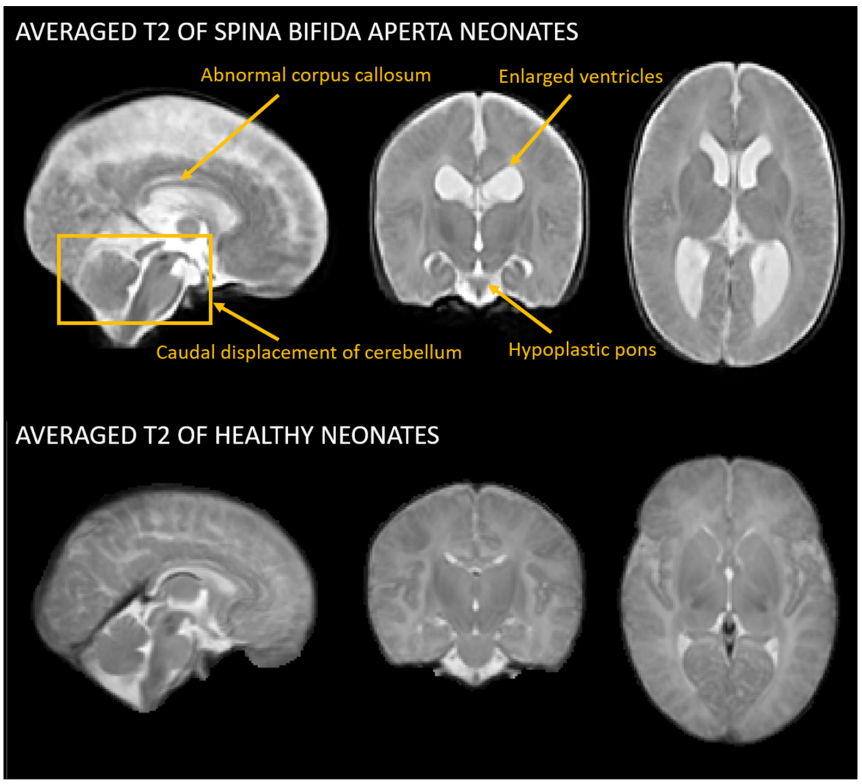


Figure 1. Characteristic anatomical differences between SBA and healthy neonates, represented by population mean template images. Some of the frequently observed SBA manifestations can be seen in the upper row: thinning of the corpus callosum, enlargement of the ventricles and hypoplastic pons, and caudally dislocated cerebellum, compared to a healthy developing neonate (bottom row). The T2-weighted images are the templates of the OSBA and ENA33 atlas, respectively.

2. Data Description

2.1. Template Images and Tissue Prior Maps

All image files are stored in 64-bit floating-point precision NIFTI-1+ images, gzip compressed. The OSBA atlas includes a T2-weighted template image with an image resolution of and size of 117 × 159 × 126 with isotropic voxel dimensions of 0.85 mm and a corresponding fractional anisotropy template with identical image dimensions (Table 1). The following tissue priors are included in the atlas: background, extra-cerebral fluid spaces, cortical gray matter, white matter, ventricles, deep gray matter structures, hippocampus, brainstem, and cerebellum (Figure 2). The tissue prior maps were normalized to obtain a value between 0 and 1.

Table 1. List of files in the OSBA atlas.

File Path and Name	Description
./Documentation/	
OSBA_10_ROITable_ENA33_Connectomic.csv	ROI information (e.g., nodes for connectomic analysis)
OSBA_10_ROITable_ENA33.csv	ROI information
./Labels/	
OSBA_10_Labels_Brain.nii.gz	Brain mask
OSBA_10_Labels_ENA33.nii.gz	ROI system, based on the adaptation of the ENA33 labels to the SBA brain
OSBA_10_Labels_ENA33_Connectomic.nii.gz	ROI system for connectomic analysis (ventricles and corpus callosum excluded)

Table 1. *Cont.*

File Path and Name	Description
OSBA_10_Labels_WMSkeleton.nii.gz	White matter skeleton for TBSS analysis
OSBA_10_Labels_WMSkeleton_thresholded.nii.gz	White matter skeleton for TBSS analysis, thresholded
./Templates/	
OSBA_10_FA_template.nii.gz	Fractional anisotropy template image
OSBA_10_T2_template.nii.gz	T2-weighted template image
./Tissuepriors	
OSBA_10_Prior_Background.nii.gz	Tissue prior map, background
OSBA_10_Prior_Brainstem.nii.gz	Tissue prior map, brainstem
OSBA_10_Prior_Cerebellum.nii.gz	Tissue prior map, cerebellum
OSBA_10_Prior_Cortex.nii.gz	Tissue prior map, cerebral cortex
OSBA_10_Prior_Hippocampus.nii.gz	Tissue prior map, hippocampus
OSBA_10_Prior_Ventricle.nii.gz	Tissue prior map, ventricles
OSBA_10_Prior_WM.nii.gz	Tissue prior map, white matter
OSBA_10_Prior_dGM.nii.gz	Tissue prior map, deep gray matter structures
OSBA_10_Prior_eCSF.nii.gz	Tissue prior map, extra-axial cerebrospinal fluid

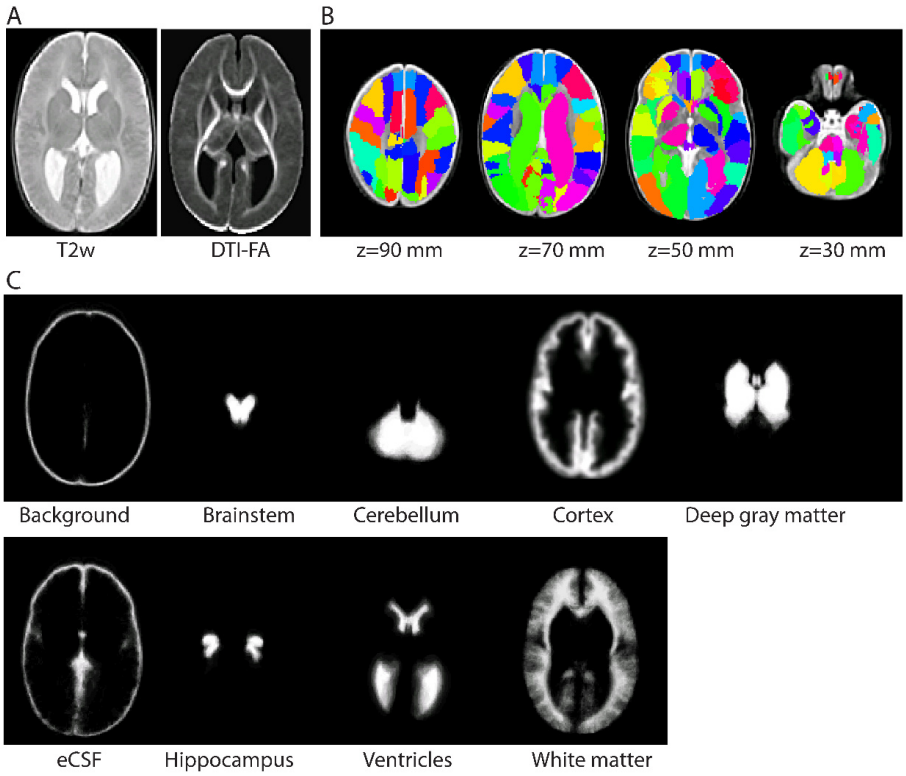


Figure 2. Templates, ROI system and anatomical priors included in the OSBA atlas. (**A**) axial cross-section of the T2-weighted and fractional anisotropy anatomical templates, (**B**) ROI label maps at different axial cross-sectional views, and (**C**) anatomical prior maps.

2.2. Regions of Interest (ROI)

Due to the characteristic anatomical configuration of the brain with SBA, the adaptation of ROIs determined from normal subjects is a challenging task. In the SBA atlas, several modifications were made to fit the anatomy of the template images (see Section 3.5). A recent adaptation of the AAL anatomical ontologies was used by adapting the labels from the publicly available ENA33 atlas to the SBA brain [10]. We include a modified version ('connectomic' atlas) of this ROI system in which the labels corresponding to the lateral ventricles and corpus callosum were removed. The label names, spatial coordinates, and volumes are detailed in Tables A1 and A2.

3. Methods

3.1. MRI Acquisitions

During the neonatal MRI acquisitions, all infants were sedated. Ear protection (earplugs and Minimuffs) was used, oxygen saturation and heart rate were monitored, and all examinations were supervised by a neonatologist or a neonatal nurse. A structural MRI was acquired with fast spin-echo T2-weighted FSE anatomical sequences in axial, coronal, and FRFSE sequences in the sagittal planes on either a 1.5 T MRI scanner (GE Healthcare, Signa Discovery MR450, Milwaukee, WI, USA) or a 3.0 T MRI scanner using an 8-channel head coil (GE Healthcare, Signa Discovery MR750, Milwaukee, WI, USA). A total of 9 infants were scanned on the 1.5 T MRI, while 19 were scanned on the 3.0 T MRI. The scanning parameters were the following.

A T2-weighted MRI was performed in axial, coronal, and sagittal planes for the 1.5 T sequence using the following parameters: 4400–4575 ms (variable), TE: 101–105 ms (variable), flip angle: 160°, field of view (FOV): 180 mm, acquisition matrix: 320 × 256 (70% sampling); resampled in-plane resolution was 0.35 × 0.35 mm, and slice thickness: 2.5 mm with a 0.2 mm slice gap. For the 3.0 T sequence, a T2-weighted MRI was acquired in the axial plane with TR: 7800–7900 ms (variable), TE: 101–105 ms (variable), flip angle: 111°. FOV: 180 mm, and acquisition matrix: 384 × 320 (70% sampling); resampled in-plane resolution was 0.35 × 0.35 mm, and slice thickness: 2.5 mm with a 0.2 mm slice gap.

Diffusion tensor imaging (DTI) was acquired in the axial plane using a pulsed gradient spin-echo echo-planar imaging (EPI) sequence. The 1.5T DTI sequence parameters are as follows: TR: 4100–4400 ms (variable), TE: 90–100 ms (variable), acquisition matrix: 128 × 128, field of view: 180 mm, and flip angle: 90°. Diffusion weighting was achieved by using 21 diffusion encoding gradient directions at a b-value of 1000 s/mm^2 and one b = 0 image. Acquisition matrix: 128 × 128, resampled in-plane resolution 0.7 × 0.7 mm, and slice thickness: 3 mm, no slice gap. The 3.0 T DTI sequence parameters were as follows: TR: 4100–4400 ms (variable), TE: 100 ms, acquisition matrix: 128 × 128, field of view: 180 mm, and flip angle: 90°. Diffusion weighting was achieved by using 35 diffusion encoding gradient directions at a b-value of 700 s/mm^2 and four b = 0 images. Acquisition matrix: 128 × 128, resampled in-plane resolution 0.7 × 0.7 mm, and slice thickness: 3 mm, no slice gap.

3.2. Subjects

An MRI was performed based on clinical indications. The criteria for undergoing prenatal repair surgery were established based on modified MOMS criteria, as outlined in previous publications authored by our research team [11,12]. The demographics of the first 150 subjects in the clinical cohort study are detailed in the publications of the clinical team [11]. For the construction of the OSBA atlas, we included MRI data of newborns who underwent surgical corrections between 2015 and 2018. The inclusion criteria were as follows: (1) excellent image quality based on visual assessment and (2) lateral ventricle width < 15 mm, measured at the trigonum level of the axial T2 MRI. This selection resulted in 28 MRI datasets used for the atlas construction.

The corrected gestational age at the time of the MRI scan was 38.1 ± 1.1 (mean ± SD, range: 35.7–40.7), and the birth weight of the infants was 2598 ± 445 g (mean ± SD, range: 1400–3350 g). The male/female ratio was 16/12. A total of 16 infants had myelomeningocele lesions (57%), while 12 had myeloschisis (43%). The (highest) anatomical levels of the spinal lesion levels were the following (case numbers): L1: 3, L2: 0, L3. 5, L4: 10, L5: 8, and S1: 2. Subependymal nodules were reported in 3 infants (10.7%).

3.3. MRI Processing

For each subject, the super-resolution slice-to-volume reconstruction algorithm SVRTK was applied to the axial, coronal, and sagittal T2 images, resulting in a 3D super-resolution reconstructed T2-weighted image (further named as a 3DT2 image) with an isotropic image

resolution of 0.4 × 0.4 × 0.4 mm [13]. As part of the image reconstruction, noise correction, bias field inhomogeneity correction, and image normalization were performed.

Next, the 3DT2 images were segmented into anatomical compartments according to the definition of the developing Human Connectome Project (dHCP) structural pipeline [14]. We utilized an in-house network based on the U-Net architecture, which was trained on 3DT2 images and ground truth image labels sampled from a population of normally developing neonatal controls and SBA data. Here, the goal was to improve the accuracy of the dHCP pipeline for neonatal brains with SBA. The training data were created in two steps. First, by running the dHCP structural pipeline on the selected normally developing controls from the dHCP dataset release v2 and SBA cases from Zürich. Next, we carried out manual corrections for cases with errors, particularly in the presence of ventricular enlargement. The network was then re-trained on the corrected dataset and further used to segment the SBA data for the OSBA atlas.

DTI was processed using an in-house script wrapping common image processing libraries. For slice-to-volume reconstruction and to correct for eddy current and head motion-induced geometric distortions, the eddy_cuda in the Functional Magnetic Imaging of the Brain Software Library (FSL) was used [15]. Next, the dtifit command in FSL was utilized for diffusion tensor and scalar maps estimation (such as fractional anisotropy—FA, B0 image, and mean diffusivity map), and scalars were estimated using weighted least squares regression.

3.4. Template Construction

The initial spatial reference of the OSBA atlas was the T2-weighted template from the ALBERTS atlas representing the average normally developing neonatal brain at the 38 corrected gestation week [16], matching the mean age at MRI of the subjects in our study.

The data to be included in the OSBA atlas were selected to represent the average ventricular dilation, excluding cases with pronounced hydrocephalus (ventricular width measured at the trigonum < 15 mm), but also selected to be of good to excellent image quality after visual assessment. First, 28 selected subjects' 3DT2 images were re-oriented to the 38-week T2-weighted template from the neonatal atlas by using 6 degrees of freedom registration with the flirt tool in FSL [15]. The neonatal template served only as a spatial reference for initial alignment and defining image dimensions.

Next, an unbiased non-linear template representative of the selected subjects was reconstructed using the Advanced Normalization Tools (ANTs) by running the multimodal template reconstruction BASH script included in the software [17,18] with default settings used for template construction.

The B0 images (intrinsically carrying T2-weighted contrast) from the DTI were transformed to the same subject's 3DT2 image using 12 degrees of freedom registration with the flirt tool in FSL. Next, we used the transformations established in the previous template construction steps to match the DTI space to the T2-weighted template's space. We transformed the FA maps to the T2-weighted template, ran the ANTs template construction script again in this canonical space using the non-linearly deformed FA maps, and the median image across all subjects was estimated to reduce the effects of data outliers, and the resulting image was saved as the FA template. A white matter skeleton was derived from this FA template by using the tbss_skeleton command implemented in FSL [19].

3.5. Anatomical Parcellation and Transformation of Common Neonatal ROIs to the OSBA Atlas

First, probabilistic maps of anatomical tissue priors were created. We saved the binary label maps corresponding to each of the segmentation labels and then transformed these using the non-linear deformation to match them to the template space. The average map was then divided by its maximum value to normalize it to obtain values between 0 and 1.

The OSBA atlas includes anatomical ROIs based on the ENA33 neonatal atlas [10]. The ENA33 comprises T2-weighted templates, which were matched to the SBA T2-weighted template. However, in this process, we noted that neither a linear nor local non-linear

registration, in which the registration metrics are globally optimized for the whole anatomical image, were able to precisely match the borders of the subcortical tissues between the anatomical template of the ENA33 and the SBA atlas. This was mainly attributed to the enlarged ventricles and the characteristic shape of the lateral ventricles and brainstem. Therefore, we split the ROIs into groups corresponding to the cortex, subcortical gray matter structures, and other structures.

All cortical ROIs were transformed from the ENA33 to the SBA by non-linear registration matching the probability maps corresponding to the gray matter. Subcortical ROIs, due to the adjacency to the dilated ventricles, were first automatically, then manually registered to the SBA template separately in the following three groups: the bilateral caudate nucleus (label 71,72), cingulate ROIs (labels 31–36), and ROIs corresponding to the thalamus, pallidum, putamen, and hippocampus. These registrations were carried out using the Slicer 3D software with 6 degrees of freedom registration, and the registration accuracy was visually controlled [20]. The rest of the ROIs were transformed to the SBA by image-based (global) registrations guided by matching the T2-weighted templates in both atlases. After this procedure, the ROIs were combined into a single-label map.

3.6. Superiority of the OSBA Atlas for the Spatial Normalization of T2 Images of Newborns with SBA

Spatial normalization of subjects for voxel-level statistical analysis, ROI-based statistics, or connectomic analysis needs high spatial precision. To demonstrate the superiority of the OSBA atlas, we aligned a subject's native T2-weighted MR image to the OSBA template and the ENA33 template. The ROI alignment is insufficient in the ENA33 atlas due to the enlarged and characteristically shaped ventricles in SBA. Our atlas allowed a better match with the observed ROIs. Figure 3 shows a comparison of how the ENA33 atlas and the OSBA atlas align with a T2 image of an SBA neonate.

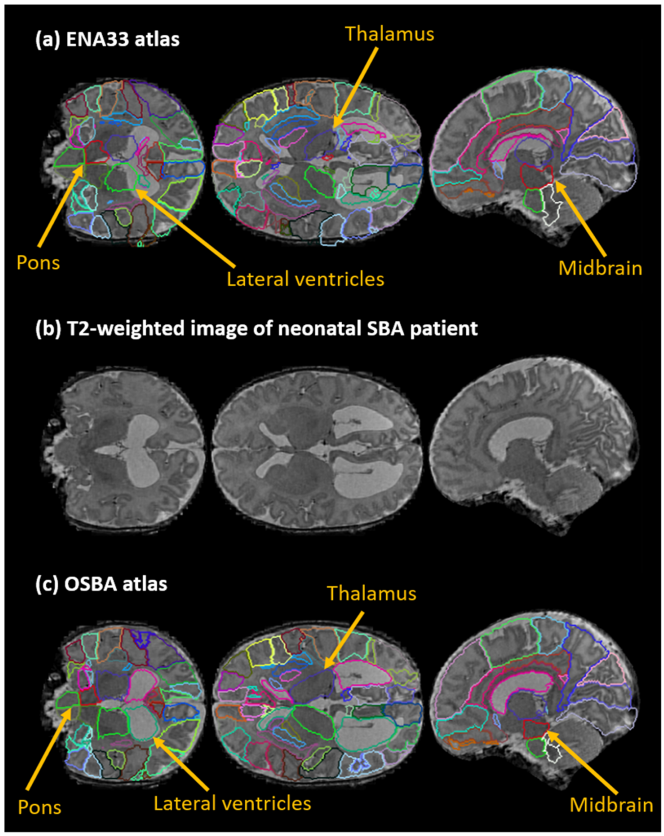


Figure 3. Demonstration of the inability to match spina bifida brains to a neonatal template created from MRI of normally developing infants. Non-linear registration results from the ENA33 atlas to the

T2-weighted subject space show mismatch, especially in the ventricles, thalamus, and partial misalignment of the midbrain and pons compared to the OSBA atlas. Notes. Using the diffeomorphic symmetric image normalization method (SyN) in ANTs, the corresponding T2-weighted template image of the atlases was registered as the SBA subject's T2-weighted image.

3.7. Limitations

The MRI data utilized in the OSBA atlas is restricted to the early neonatal period because MRI scans were clinically indicated during this age range. Consequently, there is no opportunity for a cross-sectional representation of early brain development, as in our clinic, MRI is acquired at one neonatal time point, preferably within 2 to 4 weeks after birth. A further limitation is that the OSBA atlas only contains asymmetric templates and tissue priors. Future works should establish symmetric templates for less biased analysis of left-right asymmetries in the brain with SBA. The OSBA atlas falls short of capturing the variability present in brains affected by SBA. Conditional atlas generation methods have the capacity to represent the diverse anatomical variations observed in SBA. In the context of SBA, this would mean the different grades of ventriculomegaly, Chiari-II grade, and the presence of various forms of corpus callosum abnormalities associated with SBA. Currently, we excluded cases with severe ventriculomegaly due to the difficulties in co-registering them with images of mild or moderate ventriculomegaly. However, future versions of the OSBA atlas might include such representations of such variability in SBA. While we have shown the limitations of a non-spina bifida-specific neonatal atlas (ENA33) in aligning T2 images of spina bifida subjects, further systematic experiments should be conducted to better demonstrate the advantages of the OSBA atlas. The OSBA atlas is limited to two MRI sequences, T2-weighted and diffusion tensor imaging. The data source we used is limited by the fact that we used a mixture of data acquired on a 1.5T and 3.0T clinical scanner. Furthermore, the DTI dataset used did not undergo geometric distortion correction by means of topup or similar algorithms since our clinical protocol only used a one-phase-encoding direction when acquiring the B0 images. Future work is needed with improved imaging sequences and templates created for the various field strengths of DTI sequence variations.

Author Contributions: Conceptualization, A.S. and A.J.; methodology, A.S. and A.J.; software, A.S. and A.J.; validation, A.S., K.P. and A.J.; formal analysis, A.S. and A.J.; investigation, A.S. and A.J.; resources, L.M., B.P., U.M., K.P., P.G., R.K., S.B.S.G.Z. and A.J.; data curation, S.A., H.J. and A.J.; writing—original draft preparation, A.S., K.P. and A.J.; writing—review and editing, A.S., H.J., L.M., B.P., U.M. and A.J.; visualization, A.S. and A.J.; supervision, A.J.; project administration, A.J.; funding acquisition, A.J. All authors have read and agreed to the published version of the manuscript.

Funding: This research was funded by the University Research Priority Program (URPP) 'Adaptive Brain Circuits in Development and Learning (AdaBD)' of the University of Zurich, the Prof. Dr. Max Cloetta Foundation, the EMDO Foundation, and the Vontobel Foundation.

Institutional Review Board Statement: All parents or caregivers gave written informed consent for the further use of their infants' data in research. The study was conducted in accordance with the Declaration of Helsinki and approved by the Ethics Committee of the Canton of Zurich for collecting and analyzing data retrospectively (decision numbers: 2016-01019, 2021-01101, and 2022-0115).

Informed Consent Statement: Informed consent was obtained from all subjects involved in the study.

Data Availability Statement: The data presented in this study are available on Zenodo at the request of the corresponding author due to restrictions imposed to ensure compliance with research ethics and data privacy regulations.

Acknowledgments: The authors want to first thank all families who participated in this research. Infrastructure support for this research was provided by the Clinical Trial Center, University Hospital of Zurich. The authors want to first thank all families who participated in this research. In addition, we thank our contributing study group, without whom this research would not have been possible. From the University Children's Hospital this includes Barbara Casanova, Ruth Etter, Patrice Grehten, Domenic Grisch, Cornelia Hagmann, Mirjam Harm, Maya Horst Luethy, Jenny Kienzler,

Raimund Kottke, Niklaus Krayenbuehl, Markus A. Landolt, Bea Latal Hajnal; Andreas Meyer-Heim, Theres Moehrlen, Svea Muehlberg, Evelyne Riesen, Brigitte Seliner, Mithula Shellvarajah, Alexandra Wattinger and Noemi Zweifel. From the University Hospital Zurich, our study group consists of Lukas Kandler, Nicole Ochsenbein, Nele Struebing, Max Antonio Thomasius, and Ladina Vonzun. Infrastructure support for this research was provided by the Clinical Trial Center, University Hospital of Zurich.

Conflicts of Interest: The authors declare no conflicts of interest. The funders had no role in the design of the study, in the collection, analyses, or interpretation of data, in the writing of the manuscript, or in the decision to publish the results.

Appendix A

Table A1. ROI information of the OSBA atlas.

Label	Label Name	COG [1] in Voxel Dimensions			COG [1] in mm Dimensions			Volume in mm^3	
		x	y	z	x	y	z	OSBA	ENA33
1	Precentral_L	85.543	86.576	88.759	−21.951	−9.770	37.558	11,166	10,257
2	Precentral_R	32.970	90.215	88.389	23.229	−6.643	37.240	11,029	10,403
3	Frontal_Sup_L	72.947	115.517	82.997	−11.126	15.101	32.607	13,462	11,547
4	Frontal_Sup_R	46.372	119.390	79.514	11.712	18.429	29.613	11,290	10,134
5	Frontal_Sup_Orb_L	68.917	122.058	39.058	−7.663	20.721	−5.154	2134	1824
6	Frontal_Sup_Orb_R	50.279	120.012	38.082	8.354	18.963	−5.992	1983	1668
7	Frontal_Mid_L	83.561	113.941	75.008	−20.248	13.746	25.741	15,545	13,495
8	Frontal_Mid_R	35.854	115.685	75.964	20.750	15.245	26.563	16,746	15,345
9	Frontal_Mid_Orb_L	76.690	128.197	42.521	−14.343	25.998	−2.177	3193	2635
10	Frontal_Mid_Orb_R	41.864	127.568	42.813	15.586	25.457	−1.926	3237	2902
11	Frontal_Inf_Oper_L	90.597	101.307	63.473	−26.294	2.889	15.828	3671	3332
12	Frontal_Inf_Oper_R	27.712	103.866	62.958	27.748	5.088	15.386	3695	3367
13	Frontal_Inf_Tri_L	89.779	113.174	57.294	−25.591	13.087	10.518	3793	3392
14	Frontal_Inf_Tri_R	28.135	115.343	57.695	27.384	14.951	10.863	4082	3727
15	Frontal_Inf_Orb_L	82.036	111.898	42.482	−18.937	11.991	−2.210	5958	6071
16	Frontal_Inf_Orb_R	36.759	113.415	42.396	19.973	13.294	−2.285	4928	4887
17	Rolandic_Oper_L	93.084	81.361	66.223	−28.432	−14.253	18.192	7764	6556
18	Rolandic_Oper_R	25.235	84.754	67.886	29.876	−11.337	19.621	6111	4549
19	Supp_Motor_Area_L	64.366	94.133	96.885	−3.752	−3.276	44.542	7037	7196
20	Supp_Motor_Area_R	53.794	95.604	96.514	5.334	−2.012	44.223	5880	6663
21	Olfactory_L	65.126	100.927	41.292	−4.405	2.562	−3.234	1665	1543
22	Olfactory_R	53.974	101.550	41.781	5.178	3.097	−2.813	1818	1630
23	Frontal_Sup_Medial_L	64.617	127.752	71.887	−3.968	25.615	23.059	7932	7133
24	Frontal_Sup_Medial_R	54.444	127.603	71.539	4.775	25.487	22.760	8383	8390
25	Frontal_Med_Orb_L	63.617	122.037	47.188	−3.108	20.703	1.834	3836	1990
26	Frontal_Med_Orb_R	54.542	124.243	45.045	4.690	22.599	−0.008	3262	1973
27	Rectus_L	64.399	117.876	36.548	−3.781	17.128	−7.311	1603	1354
28	Rectus_R	55.203	118.714	36.443	4.122	17.848	−7.400	1457	1301
29	Insula_L	82.997	94.258	53.186	−19.763	−3.169	6.988	3757	4901
30	Insula_R	31.986	95.366	53.804	24.074	−2.217	7.519	2026	4501
31	Cingulum_Ant_L	62.574	111.255	69.403	−2.212	11.438	20.924	2393	3089
32	Cingulum_Ant_R	55.256	113.158	63.890	4.077	13.073	16.186	3036	3003
33	Cingulum_Mid_L	62.440	71.317	84.300	−2.097	−22.884	33.727	3654	4472
34	Cingulum_Mid_R	52.928	71.652	84.377	6.077	−22.596	33.793	3651	4816
35	Cingulum_Post_L	61.136	56.598	72.407	−0.976	−35.533	23.506	199	454
36	Cingulum_Post_R	55.820	57.753	74.127	3.592	−34.541	24.984	267	565
37	Hippocampus_L	77.737	77.931	40.158	−15.242	−17.200	−4.208	1732	2658
38	Hippocampus_R	40.475	80.128	41.675	16.780	−15.312	−2.904	2073	2793
39	ParaHippocampal_L	74.656	80.363	34.580	−12.595	−15.110	−9.002	2407	3193
40	ParaHippocampal_R	43.663	82.537	34.942	14.039	−13.241	−8.691	2313	3039
41	Amygdala_L	76.662	89.686	36.916	−14.319	−7.098	−6.994	509	821
42	Amygdala_R	39.625	92.468	38.109	17.510	−4.707	−5.969	523	963
43	Calcarine_L	61.944	27.103	62.783	−1.671	−60.880	15.235	5354	5546
44	Calcarine_R	50.685	32.047	64.413	8.005	−56.631	16.636	5457	5189
45	Cuneus_L	64.107	29.395	78.938	−3.530	−58.911	29.119	5099	4541
46	Cuneus_R	49.818	33.323	79.395	8.751	−55.535	29.511	5047	4394
47	Lingual_L	65.725	31.759	48.574	−4.920	−56.879	3.024	9004	9341
48	Lingual_R	48.215	33.355	49.769	10.128	−55.507	4.051	10,212	9726
49	Occipital_Sup_L	73.440	30.657	80.139	−11.550	−57.826	30.151	3126	2780
50	Occipital_Sup_R	41.154	28.882	78.842	16.196	−59.352	29.036	4698	4221
51	Occipital_Mid_L	79.339	26.437	69.128	−16.619	−61.453	20.688	7811	7164
52	Occipital_Mid_R	31.690	33.049	69.240	24.329	−55.770	20.785	8067	7933
53	Occipital_Inf_L	83.249	26.610	50.274	−19.980	−61.304	4.486	4258	4156
54	Occipital_Inf_R	30.633	30.554	51.783	25.237	−57.914	5.783	7272	6727
55	Fusiform_L	80.795	57.900	37.179	−17.871	−34.414	−6.768	6442	6906
56	Fusiform_R	35.314	58.065	39.493	21.214	−34.272	−4.780	5727	6407

Table A1. *Cont.*

Label	Label Name	COG [1] in Voxel Dimensions			COG [1] in mm Dimensions			Volume in mm^3	
		x	y	z	x	y	z	OSBA	ENA33
57	Postcentral_L	86.510	73.361	91.951	−22.782	−21.127	40.302	9347	8252
58	Postcentral_R	31.164	76.934	92.571	24.781	−18.057	40.834	9599	8597
59	Parietal_Sup_L	76.020	49.592	97.510	−13.767	−41.554	45.079	7570	6655
60	Parietal_Sup_R	42.249	51.269	99.056	15.255	−40.112	46.407	6198	5583
61	Parietal_Inf_L	87.763	55.315	88.647	−23.859	−36.636	37.462	2966	2872
62	Parietal_Inf_R	30.081	59.050	88.504	25.712	−33.426	37.339	8400	7008
63	SupraMarginal_L	95.107	62.319	79.087	−30.170	−30.617	29.246	5555	4723
64	SupraMarginal_R	19.688	65.960	79.010	34.643	−27.487	29.180	4253	3580
65	Angular_L	87.365	42.717	81.493	−23.516	−47.462	31.314	4229	4237
66	Angular_R	26.293	45.882	79.961	28.967	−44.742	29.998	2794	2729
67	Precuneus_L	63.791	47.390	87.647	−3.258	−43.446	36.603	9210	8884
68	Precuneus_R	52.067	48.190	87.674	6.817	−42.759	36.626	8976	8573
69	Paracentral_Lobule_L	63.869	67.299	102.016	−3.325	−26.337	48.951	2960	2733
70	Paracentral_Lobule_R	52.008	71.244	102.542	6.868	−22.946	49.403	4133	3867
71	Caudate_L	69.778	100.837	55.905	−8.403	2.485	9.324	693	1362
72	Caudate_R	48.189	103.485	55.091	10.151	4.761	8.625	870	1449
73	Putamen_L	77.168	95.553	52.274	−14.754	−2.056	6.205	1782	1995
74	Putamen_R	37.948	98.198	53.344	18.951	0.217	7.124	2077	2334
75	Pallidum_L	72.988	94.696	50.770	−11.162	−2.792	4.912	1652	1801
76	Pallidum_R	43.154	96.604	50.989	14.477	−1.153	5.100	1712	1910
77	Thalamus_L	69.029	77.262	57.078	−7.759	−17.775	10.333	5915	4967
78	Thalamus_R	47.634	79.562	57.623	10.627	−15.798	10.801	5825	5095
79	Heschl_L	89.732	74.852	60.298	−25.551	−19.846	13.100	1293	1263
80	Heschl_R	28.961	79.100	61.322	26.674	−16.196	13.980	1214	1134
81	Temporal_Sup_L	95.094	68.860	58.463	−30.159	−24.995	11.522	8851	7889
82	Temporal_Sup_R	22.367	76.721	58.030	32.341	−18.239	11.151	9445	8941
83	Temporal_Pole_Sup_L	89.355	95.144	37.500	−25.227	−2.408	−6.492	3254	3193
84	Temporal_Pole_Sup_R	29.844	98.693	37.927	25.915	0.642	−6.125	2600	3424
85	Temporal_Mid_L	93.988	56.891	54.219	−29.209	−35.282	7.876	9974	9265
86	Temporal_Mid_R	22.072	66.520	52.941	32.595	−27.006	6.778	11,112	10,498
87	Temporal_Pole_Mid_L	87.198	94.812	26.667	−23.373	−2.693	−15.802	1310	1698
88	Temporal_Pole_Mid_R	32.747	97.307	25.565	23.421	−0.548	−16.749	774	1524
89	Temporal_Inf_L	91.913	61.356	39.051	−27.425	−31.444	−5.159	10,160	9878
90	Temporal_Inf_R	25.423	68.582	36.859	29.714	−25.234	−7.043	8351	7681
91	CorpusCallosum	57.581	85.064	73.483	2.079	−11.070	24.431	4330	3562
92	Lateral_Ventricle_L	72.414	68.197	65.837	−10.668	−25.565	17.860	27,034	3228
93	Lateral_Ventricle_R	43.415	70.915	66.878	14.252	−23.230	18.755	22,297	3361
94	Midbrain_L	63.015	72.828	42.660	−2.591	−21.585	−2.058	1854	2341
95	Midbrain_R	54.308	73.016	42.968	4.891	−21.423	−1.793	1707	2331
96	Pons_L	62.511	72.080	29.032	−2.158	−22.228	−13.770	1007	1067
97	Pons_R	54.973	71.696	28.977	4.320	−22.558	−13.817	1212	1347
98	Medulla_L	63.423	61.522	23.212	−2.942	−31.301	−18.771	2113	2582
99	Medulla_R	55.003	61.331	22.581	4.294	−31.466	−19.313	2369	3044
100	Cerebelum_L	71.631	48.908	28.988	−9.995	−42.142	−13.807	11,410	13,721
101	Cerebelum_R	44.934	49.781	29.499	12.947	−41.392	−13.368	11,423	13,704
102	Vermis_Ant_L	59.958	53.432	39.882	0.036	−38.254	−4.445	542	935
103	Vermis_Ant_R	56.278	53.478	40.116	3.199	−38.214	−4.244	508	914
104	Vermis_Post_L	63.180	47.630	31.171	−2.733	−43.240	−11.931	1680	2353
105	Vermis_Post_R	54.301	47.333	31.114	4.897	−43.495	−11.980	1470	2297
106	Vermis_Cent_L	62.153	51.094	24.805	−1.850	−40.263	−17.402	615	880
107	Vermis_Cent_R	54.236	52.135	24.390	4.953	−39.369	−17.759	728	1053

[1] COG = center of gravity.

Table A2. ROI information of the connectomic OSBA atlas.

Label	Label Name	COG [1] in Voxel Dimensions			COG [1] in mm Dimensions			Volume in mm^3	
		x	y	z	x	y	z	OSBA	ENA33
1	Precentral_L	85.543	86.576	88.759	−21.951	−9.770	37.558	11,166	10,257
2	Precentral_R	32.970	90.215	88.389	23.229	−6.643	37.240	11,029	10,403
3	Frontal_Sup_L	72.947	115.517	82.997	−11.126	15.101	32.607	13,462	11,547
4	Frontal_Sup_R	46.372	119.390	79.514	11.712	18.429	29.613	11,290	10,134
5	Frontal_Sup_Orb_L	68.917	122.058	39.058	−7.663	20.721	−5.154	2134	1824
6	Frontal_Sup_Orb_R	50.279	120.012	38.082	8.354	18.963	−5.992	1983	1668
7	Frontal_Mid_L	83.561	113.941	75.008	−20.248	13.746	25.741	15,545	13,495
8	Frontal_Mid_R	35.854	115.685	75.964	20.750	15.245	26.563	16,746	15,345
9	Frontal_Mid_Orb_L	76.690	128.197	42.521	−14.343	25.998	−2.177	3193	2635
10	Frontal_Mid_Orb_R	41.864	127.568	42.813	15.586	25.457	−1.926	3237	2902
11	Frontal_Inf_Oper_L	90.597	101.307	63.473	−26.294	2.889	15.828	3671	3332
12	Frontal_Inf_Oper_R	27.712	103.866	62.958	27.748	5.088	15.386	3695	3367
13	Frontal_Inf_Tri_L	89.779	113.174	57.294	−25.591	13.087	10.518	3793	3392
14	Frontal_Inf_Tri_R	28.135	115.343	57.695	27.384	14.951	10.863	4082	3727
15	Frontal_Inf_Orb_L	82.036	111.898	42.482	−18.937	11.991	−2.210	5958	6071

Table A2. *Cont.*

Label	Label Name	COG [1] in Voxel Dimensions			COG [1] in mm Dimensions			Volume in mm^3	
		x	y	z	x	y	z	OSBA	ENA33
16	Frontal_Inf_Orb_R	36.759	113.415	42.396	19.973	13.294	−2.285	4928	4887
17	Rolandic_Oper_L	93.084	81.361	66.223	−28.432	−14.253	18.192	7764	6556
18	Rolandic_Oper_R	25.235	84.754	67.886	29.876	−11.337	19.621	6111	4549
19	Supp_Motor_Area_L	64.366	94.133	96.885	−3.752	−3.276	44.542	7037	7196
20	Supp_Motor_Area_R	53.794	95.604	96.514	5.334	−2.012	44.223	5880	6663
21	Olfactory_L	65.126	100.927	41.292	−4.405	2.562	−3.234	1665	1543
22	Olfactory_R	53.974	101.550	41.781	5.178	3.097	−2.813	1818	1630
23	Frontal_Sup_Medial_L	64.617	127.752	71.887	−3.968	25.615	23.059	7932	7133
24	Frontal_Sup_Medial_R	54.444	127.603	71.539	4.775	25.487	22.760	8383	8390
25	Frontal_Med_Orb_L	63.617	122.037	47.188	−3.108	20.703	1.834	3836	1990
26	Frontal_Med_Orb_R	54.542	124.243	45.045	4.690	22.599	−0.008	3262	1973
27	Rectus_L	64.399	117.876	36.548	−3.781	17.128	−7.311	1603	1354
28	Rectus_R	55.203	118.714	36.443	4.122	17.848	−7.400	1457	1301
29	Insula_L	82.997	94.258	53.186	−19.763	−3.169	6.988	3757	4901
30	Insula_R	31.986	95.366	53.804	24.074	−2.217	7.519	2026	4501
31	Cingulum_Ant_L	62.574	111.255	69.403	−2.212	11.438	20.924	2393	3089
32	Cingulum_Ant_R	55.256	113.158	63.890	4.077	13.073	16.186	3036	3003
33	Cingulum_Mid_L	62.440	71.317	84.300	−2.097	−22.884	33.727	3654	4472
34	Cingulum_Mid_R	52.928	71.652	84.377	6.077	−22.596	33.793	3651	4816
35	Cingulum_Post_L	61.136	56.598	72.407	−0.976	−35.533	23.506	199	454
36	Cingulum_Post_R	55.820	57.753	74.127	3.592	−34.541	24.984	267	565
37	Hippocampus_L	77.737	77.931	40.158	−15.242	−17.200	−4.208	1732	2658
38	Hippocampus_R	40.475	80.128	41.675	16.780	−15.312	−2.904	2073	2793
39	ParaHippocampal_L	74.656	80.363	34.580	−12.595	−15.110	−9.002	2407	3193
40	ParaHippocampal_R	43.663	82.537	34.942	14.039	−13.241	−8.691	2313	3039
41	Amygdala_L	76.662	89.686	36.916	−14.319	−7.098	−6.994	509	821
42	Amygdala_R	39.625	92.468	38.109	17.510	−4.707	−5.969	523	963
43	Calcarine_L	61.944	27.103	62.783	−1.671	−60.880	15.235	5354	5546
44	Calcarine_R	50.685	32.047	64.413	8.005	−56.631	16.636	5457	5189
45	Cuneus_L	64.107	29.395	78.938	−3.530	−58.911	29.119	5099	4541
46	Cuneus_R	49.818	33.323	79.395	8.751	−55.535	29.511	5047	4394
47	Lingual_L	65.725	31.759	48.574	−4.920	−56.879	3.024	9004	9341
48	Lingual_R	48.215	33.355	49.769	10.128	−55.507	4.051	10,212	9726
49	Occipital_Sup_L	73.440	30.657	80.139	−11.550	−57.826	30.151	3126	2780
50	Occipital_Sup_R	41.154	28.882	78.842	16.196	−59.352	29.036	4698	4221
51	Occipital_Mid_L	79.339	26.437	69.128	−16.619	−61.453	20.688	7811	7164
52	Occipital_Mid_R	31.690	33.049	69.240	24.329	−55.770	20.785	8067	7933
53	Occipital_Inf_L	83.249	26.610	50.274	−19.980	−61.304	4.486	4258	4156
54	Occipital_Inf_R	30.633	30.554	51.783	25.237	−57.914	5.783	7272	6727
55	Fusiform_L	80.795	57.900	37.179	−17.871	−34.414	−6.768	6442	6906
56	Fusiform_R	35.314	58.065	39.493	21.214	−34.272	−4.780	5727	6407
57	Postcentral_L	86.510	73.361	91.951	−22.782	−21.127	40.302	9347	8252
58	Postcentral_R	31.164	76.934	92.571	24.781	−18.057	40.834	9599	8597
59	Parietal_Sup_L	76.020	49.592	97.510	−13.767	−41.554	45.079	7570	6655
60	Parietal_Sup_R	42.249	51.269	99.056	15.255	−40.112	46.407	6198	5583
61	Parietal_Inf_L	87.763	55.315	88.647	−23.859	−36.636	37.462	2966	2872
62	Parietal_Inf_R	30.081	59.050	88.504	25.712	−33.426	37.339	8400	7008
63	SupraMarginal_L	95.107	62.319	79.087	−30.170	−30.617	29.246	5555	4723
64	SupraMarginal_R	19.688	65.960	79.010	34.643	−27.487	29.180	4253	3580
65	Angular_L	87.365	42.717	81.493	−23.516	−47.462	31.314	4229	4237
66	Angular_R	26.293	45.882	79.961	28.967	−44.742	29.998	2794	2729
67	Precuneus_L	63.791	47.390	87.647	−3.258	−43.446	36.603	9210	8884
68	Precuneus_R	52.067	48.190	87.674	6.817	−42.759	36.626	8976	8573
69	Paracentral_Lobule_L	63.869	67.299	102.016	−3.325	−26.337	48.951	2960	2733
70	Paracentral_Lobule_R	52.008	71.244	102.542	6.868	−22.946	49.403	4133	3867
71	Caudate_L	69.778	100.837	55.905	−8.403	2.485	9.324	693	1362
72	Caudate_R	48.189	103.485	55.091	10.151	4.761	8.625	870	1449
73	Putamen_L	77.168	95.553	52.274	−14.754	−2.056	6.205	1782	1995
74	Putamen_R	37.948	98.198	53.344	18.951	0.217	7.124	2077	2334
75	Pallidum_L	72.988	94.696	50.770	−11.162	−2.792	4.912	1652	1801
76	Pallidum_R	43.154	96.604	50.989	14.477	−1.153	5.100	1712	1910
77	Thalamus_L	69.029	77.262	57.078	−7.759	−17.775	10.333	5915	4967
78	Thalamus_R	47.634	79.562	57.623	10.627	−15.798	10.801	5825	5095
79	Heschl_L	89.732	74.852	60.298	−25.551	−19.846	13.100	1293	1263
80	Heschl_R	28.961	79.100	61.322	26.674	−16.196	13.980	1214	1134
81	Temporal_Sup_L	95.094	68.860	58.463	−30.159	−24.995	11.522	8851	7889
82	Temporal_Sup_R	22.367	76.721	58.030	32.341	−18.239	11.151	9445	8941
83	Temporal_Pole_Sup_L	89.355	95.144	37.500	−25.227	−2.408	−6.492	3254	3193
84	Temporal_Pole_Sup_R	29.844	98.693	37.927	25.915	0.642	−6.125	2600	3424
85	Temporal_Mid_L	93.988	56.891	54.219	−29.209	−35.282	7.876	9974	9265
86	Temporal_Mid_R	22.072	66.520	52.941	32.595	−27.006	6.778	11,112	10,498
87	Temporal_Pole_Mid_L	87.198	94.812	26.667	−23.373	−2.693	−15.802	1310	1698
88	Temporal_Pole_Mid_R	32.747	97.307	25.565	23.421	−0.548	−16.749	774	1524
89	Temporal_Inf_L	91.913	61.356	39.051	−27.425	−31.444	−5.159	10,160	9878
90	Temporal_Inf_R	25.423	68.582	36.859	29.714	−25.234	−7.043	8351	7681
91	Midbrain_L	63.015	72.828	42.660	−2.591	−21.585	−2.058	1854	2341
92	Midbrain_R	54.308	73.016	42.968	4.891	−21.423	−1.793	1707	2331

Table A2. *Cont.*

Label	Label Name	COG [1] in Voxel Dimensions			COG [1] in mm Dimensions			Volume in mm^3	
		x	y	z	x	y	z	OSBA	ENA33
93	Pons_L	62.511	72.080	29.032	−2.158	−22.228	−13.770	1007	1067
94	Pons_R	54.973	71.696	28.977	4.320	−22.558	−13.817	1212	1347
95	Medulla_L	63.423	61.522	23.212	−2.942	−31.301	−18.771	2113	2582
96	Medulla_R	55.003	61.331	22.581	4.294	−31.466	−19.313	2369	3044
97	Cerebelum_L	71.631	48.908	28.988	−9.995	−42.142	−13.807	11,410	13,721
98	Cerebelum_R	44.934	49.781	29.499	12.947	−41.392	−13.368	11,423	13,704
99	Vermis_Ant_L	59.958	53.432	39.882	0.036	−38.254	−4.445	542	935
100	Vermis_Ant_R	56.278	53.478	40.116	3.199	−38.214	−4.244	508	914
101	Vermis_Post_L	63.180	47.630	31.171	−2.733	−43.240	−11.931	1680	2353
102	Vermis_Post_R	54.301	47.333	31.114	4.897	−43.495	−11.980	1470	2297
103	Vermis_Cent_L	62.153	51.094	24.805	−1.850	−40.263	−17.402	615	880
104	Vermis_Cent_R	54.236	52.135	24.390	4.953	−39.369	−17.759	728	1053

[1] COG = center of gravity.

References

1. Oishi, K.; Chang, L.; Huang, H. Baby Brain Atlases. *Neuroimage* **2019**, *185*, 865–880. [CrossRef] [PubMed]
2. Fidon, L.; Viola, E.; Mufti, N.; David, A.L.; Melbourne, A.; Demaerel, P.; Ourselin, S.; Vercauteren, T.; Deprest, J.; Aertsen, M. A Spatio-Temporal Atlas of the Developing Fetal Brain with Spina Bifida Aperta. *Open Res. Eur.* **2022**, *1*, 123. [CrossRef] [PubMed]
3. Evans, A.C.; Janke, A.L.; Collins, D.L.; Baillet, S. Brain Templates and Atlases. *Neuroimage* **2012**, *62*, 911–922. [CrossRef] [PubMed]
4. Ciceri, T.; Casartelli, L.; Montano, F.; Conte, S.; Squarcina, L.; Bertoldo, A.; Agarwal, N.; Brambilla, P.; Peruzzo, D. Fetal Brain MRI Atlases and Datasets: A Review. *Neuroimage* **2024**, *292*, 120603. [CrossRef] [PubMed]
5. Gholipour, A.; Rollins, C.K.; Velasco-Annis, C.; Ouaalam, A.; Akhondi-Asl, A.; Afacan, O.; Ortinau, C.M.; Clancy, S.; Limperopoulos, C.; Yang, E.; et al. A Normative Spatiotemporal MRI Atlas of the Fetal Brain for Automatic Segmentation and Analysis of Early Brain Growth. *Sci. Rep.* **2017**, *7*, 476. [CrossRef]
6. Khoshnood, B.; Loane, M.; de Walle, H.; Arriola, L.; Addor, M.-C.; Barisic, I.; Beres, J.; Bianchi, F.; Dias, C.; Draper, E.; et al. Long Term Trends in Prevalence of Neural Tube Defects in Europe: Population Based Study. *BMJ* **2015**, *351*, h5949. [CrossRef] [PubMed]
7. Schneider, J.; Mohr, N.; Aliatakis, N.; Seidel, U.; John, R.; Promnitz, G.; Spors, B.; Kaindl, A.M. Brain Malformations and Cognitive Performance in Spina Bifida. *Dev. Med. Child. Neurol.* **2021**, *63*, 295–302. [CrossRef] [PubMed]
8. Mufti, N.; Sacco, A.; Aertsen, M.; Ushakov, F.; Ourselin, S.; Thomson, D.; Deprest, J.; Melbourne, A.; David, A.L. What Brain Abnormalities Can Magnetic Resonance Imaging Detect in Foetal and Early Neonatal Spina Bifida: A Systematic Review. *Neuroradiology* **2022**, *64*, 233–245. [CrossRef] [PubMed]
9. Shrot, S.; Soares, B.P.; Whitehead, M.T. Cerebral Diffusivity Changes in Fetuses with Chiari II Malformation. *Fetal Diagn. Ther.* **2019**, *45*, 268–274. [CrossRef] [PubMed]
10. Blesa, M.; Serag, A.; Wilkinson, A.G.; Anblagan, D.; Telford, E.J.; Pataky, R.; Sparrow, S.A.; Macnaught, G.; Semple, S.I.; Bastin, M.E.; et al. Parcellation of the Healthy Neonatal Brain into 107 Regions Using Atlas Propagation through Intermediate Time Points in Childhood. *Front. Neurosci.* **2016**, *10*, 220. [CrossRef]
11. Moehrlen, U.; Ochsenbein-Kölble, N.; Stricker, S.; Moehrlen, T.; Mazzone, L.; Krähenmann, F.; Vonzun, L.; Zimmermann, R.; Meuli, M. Prenatal Spina Bifida Repair: Defendable Trespassing of MOMS Criteria Results in Commendable Personalized Medicine. *Fetal Diagn. Ther.* **2023**, *50*, 454–463. [CrossRef] [PubMed]
12. Moehrlen, U.; Ochsenbein-Kölble, N.; Mazzone, L.; Kraehenmann, F.; Hüsler, M.; Casanova, B.; Biro, P.; Wille, D.; Latal, B.; Scheer, I.; et al. Benchmarking against the MOMS Trial: Zurich Results of Open Fetal Surgery for Spina Bifida. *Fetal Diagn. Ther.* **2020**, *47*, 91–97. [CrossRef]
13. Kuklisova-Murgasova, M.; Quaghebeur, G.; Rutherford, M.A.; Hajnal, J.V.; Schnabel, J.A. Reconstruction of Fetal Brain MRI with Intensity Matching and Complete Outlier Removal. *Med. Image Anal.* **2012**, *16*, 1550–1564. [CrossRef] [PubMed]
14. Makropoulos, A.; Robinson, E.C.; Schuh, A.; Wright, R.; Fitzgibbon, S.; Bozek, J.; Counsell, S.J.; Steinweg, J.; Vecchiato, K.; Passerat-Palmbach, J.; et al. The Developing Human Connectome Project: A Minimal Processing Pipeline for Neonatal Cortical Surface Reconstruction. *Neuroimage* **2018**, *173*, 88–112. [CrossRef] [PubMed]
15. Woolrich, M.W.; Jbabdi, S.; Patenaude, B.; Chappell, M.; Makni, S.; Behrens, T.; Beckmann, C.; Jenkinson, M.; Smith, S.M. Bayesian Analysis of Neuroimaging Data in FSL. *Neuroimage* **2009**, *45*, S173–S186. [CrossRef] [PubMed]
16. Gousias, I.S.; Edwards, A.D.; Rutherford, M.A.; Counsell, S.J.; Hajnal, J.V.; Rueckert, D.; Hammers, A. Magnetic Resonance Imaging of the Newborn Brain: Manual Segmentation of Labelled Atlases in Term-Born and Preterm Infants. *Neuroimage* **2012**, *62*, 1499–1509. [CrossRef] [PubMed]
17. AVANTS, B.; EPSTEIN, C.; GROSSMAN, M.; GEE, J. Symmetric Diffeomorphic Image Registration with Cross-Correlation: Evaluating Automated Labeling of Elderly and Neurodegenerative Brain. *Med. Image Anal.* **2008**, *12*, 26–41. [CrossRef] [PubMed]
18. Avants, B.B.; Tustison, N.J.; Song, G.; Cook, P.A.; Klein, A.; Gee, J.C. A Reproducible Evaluation of ANTs Similarity Metric Performance in Brain Image Registration. *Neuroimage* **2011**, *54*, 2033–2044. [CrossRef] [PubMed]

19. Smith, S.M.; Jenkinson, M.; Johansen-Berg, H.; Rueckert, D.; Nichols, T.E.; Mackay, C.E.; Watkins, K.E.; Ciccarelli, O.; Cader, M.Z.; Matthews, P.M.; et al. Tract-Based Spatial Statistics: Voxelwise Analysis of Multi-Subject Diffusion Data. *Neuroimage* **2006**, *31*, 1487–1505. [CrossRef] [PubMed]
20. Fedorov, A.; Beichel, R.; Kalpathy-Cramer, J.; Finet, J.; Fillion-Robin, J.-C.; Pujol, S.; Bauer, C.; Jennings, D.; Fennessy, F.; Sonka, M.; et al. 3D Slicer as an Image Computing Platform for the Quantitative Imaging Network. *Magn. Reson. Imaging* **2012**, *30*, 1323–1341. [CrossRef] [PubMed]

Disclaimer/Publisher's Note: The statements, opinions and data contained in all publications are solely those of the individual author(s) and contributor(s) and not of MDPI and/or the editor(s). MDPI and/or the editor(s) disclaim responsibility for any injury to people or property resulting from any ideas, methods, instructions or products referred to in the content.